Sensors and Materials, Vol. 30, No. 3 (2018) 471–478
MYU Tokyo

S & M 1510

Resistive Switching Properties of Samarium Oxide Resistive Random Access Memories

Chien-Min Cheng,[1] Kai-Huang Chen,[2] Fuh-Cheng Jong,[1] Mei-Li Chen,[3*]
Hsuan-Hung Li,[3] Han-Chin Chen,[3] and Po-Yu Hsieh[3]

[1]Department of Electronic Engineering, Southern Taiwan University of Science and Technology,
No. 1, Nan-Tai Street, Yungkang Dist., Tainan City 710, Taiwan, R.O.C.
[2]Department of Digital Game and Animation Design, Tung Fang Design University,
No. 110, Dongfang Rd., Hunei Dist., Kaohsiung City 82941, Taiwan, R.O.C.
[3]Department of Electro-Optical Engineering, Southern Taiwan University of Science,
No. 1, Nan-Tai Street, Yungkang Dist., Tainan City 710, Taiwan, R.O.C.

(Received August 1, 2017; accepted November 2, 2017)

Keywords: RF magnetron sputtering method, resistive random access memory, samarium oxide

The bipolar switching and electrical conduction properties of the samarium oxide resistive random access memory (RRAM) device were investigated in this study. By the RF magnetron sputtering method (Sm target, RF power 75 W, chamber pressure 20 mTorr, and different oxygen concentrations), samarium oxide thin films were deposited on an indium tin oxide (ITO)/glass substrate to form a SmO_X/ITO structure. Using the metal mask and E-beam evaporation, the aluminum upper electrode was then deposited on it to form an Al/SmO_X/ITO metal/insulation/metal (MIM) structure. Additionally, conventional thermal annealing treatments were used to improve grain growth and the properties of the thin films. From the results, greater than 10^2 on/off ratio and bipolar switching cycling behaviors of two stable states were obtained. As the operating voltage is low, the conduction mechanisms for low- and high-resistance states are dominated by ohmic conduction behavior for both SET and RESET states. However, as a higher operating voltage is applied, parts of conduction mechanisms will change to space charge limit conduction behaviors. The proposed Al/SmO_X/ITO RRAM devices also exhibit good memory window and stable bipolar switching properties during 100 cycles whereas the RF power is 75 W and the oxygen concentration is 10 sccm.

1. Introduction

As the flash memory and dynamic random access memory (DRAM) are scaled down, the memories reveal charge loss and reach their limiting physical dimensions gradually.[1,2] Recently, resistive random access memory (RRAM) devices have been shown to possess advantages such as nonvolatility, high operation speed, multiple-state possibility, small bit size, and low power consumption.[3,4] Hence, RRAMs have been identified as a prospective candidate for replacing traditional memory devices, and have been widely used in portable

*Corresponding author: e-mail: cmli@stust.edu.tw
http://dx.doi.org/10.18494/SAM.2018.1766

ISSN 0914-4935 © MYU K.K.
http://myukk.org/

electronic systems, such as cellular phones, personal digital assistants (PDAs), flash storage, and digital cameras.

The basic structure of RRAMs is a dielectric layer clamped by top and bottom electrodes [metal/insulation/metal (MIM) structure]. The memory effect of RRAMs is fulfilled through the switching characteristics between a high-resistance (OFF) state (HRS) and a low-resistance (ON) state (LRS) of the dielectric layer. In the past, various materials were discovered for this dielectric layer, such as chalcogenide,(5–7) oxide-based,(8–10) carbide,(11) and amorphous silicon.(12) However, except for the above RRAM materials, samarium oxide (SmO) is another important rare-earth material owing to its high thermal stability and large band gaps. There is still insufficient information for discussing the resistive switching properties of SmO_X RRAMs to date. Hence, in this research, we investigate the resistive switching properties, bipolar switching properties, current transport mechanisms, and the on/off ratio of Al/SmO_X/indium tin oxide (ITO) RRAMs for future memory applications.

2. Experimental Procedures

With a 2 inch ITO target and different oxygen (O_2) / Argon (Ar) concentrations (O_2/Ar = 0 sccm/10 sccm, 5 sccm/10 sccm, 10 sccm/10 sccm, and 15 sccm/10 sccm), the SmO_X thin films were deposited onto the ITO/glass substrate by the RF magnetron sputtering method and with optimal deposition parameters of RF power (75 W), chamber pressure (20 mTorr), and sputtering time (10 min). Using SHIMADZU XRD-6000, the X-ray diffraction (XRD) patterns of the SmO_X thin films were recorded to determine their crystalline quality for the 2θ-degree range of 20–60°, and their surface morphologies were observed by field emission scanning electron microscopy (FE-SEM).

To complete the MIM (Al/SmO_X/ITO) structure, an array of aluminum (Al) circular top electrodes (thickness is 300 nm and diameter is 0.1 cm) was formed by E-beam evaporation in a vacuum system (5×10^{-6} Torr). The proposed Al/SmO_X/ITO RRAM devices are schematically shown in Fig. 1. The current versus applied voltage (I–V) characteristics of the Al/SmO_X/ITO RRAM were measured using a probe station and a semiconductor parameter analyzer (HP4156C). Furthermore, the number of switching cycles was measured at room temperature, and the current conduction mechanisms of SET and RESET regions were also analyzed and investigated.

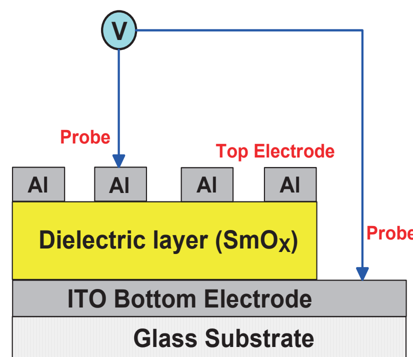

Fig. 1. (Color online) Simulated antenna gains for different distances between metal reflector and proposed antenna.

3. Results and Discussion

Figure 2 shows the XRD patterns of the as-deposited SmO_X thin films for RF power of 75 W prepared at different oxygen concentrations. From the XRD patterns, we found that all the SmO_X thin films exhibited a clear peak at about 35°, corresponding to the (400) textured orientation.[13–15] This means that completed ITO phases had been obtained according to the optimal sputtering parameters. Because argon is used to generate plasma during the sputtering process, the Ar/O_2 ratio thus can also be used to adjust the thickness of SmO_X thin films.

Figure 3 shows the FE-SEM surface morphologies of SmO_X thin films for different oxygen concentrations. It can be seen from Fig. 3(a) that nonuniform grains and pores can be found for a 0 sccm specimen. As shown in Figs. 3(b) and 3(c), the surfaces become dense as the oxygen

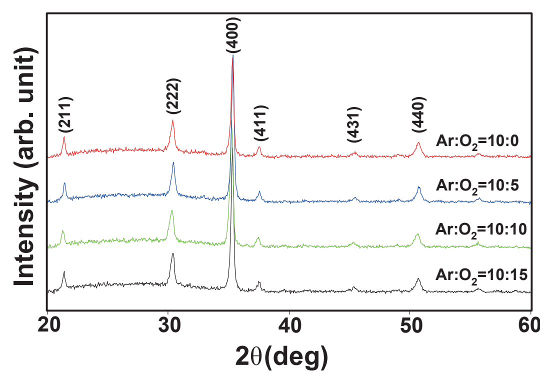

Fig. 2. (Color online) XRD patterns of the as-deposited SmO_X thin films for different oxygen concentrations.

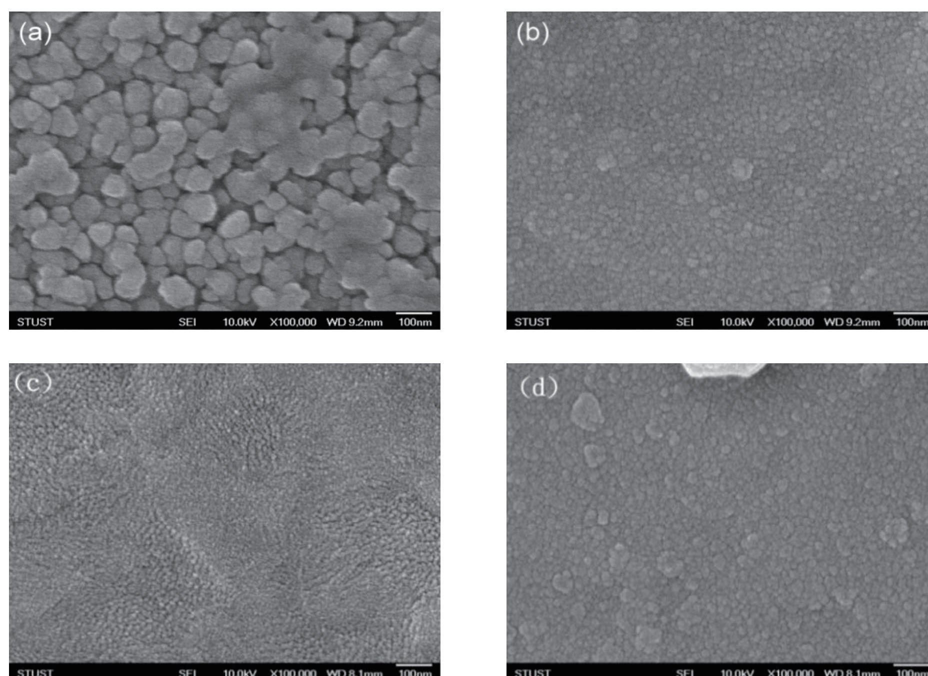

Fig. 3. Surface morphologies of SmO_X thin films for different oxygen concentrations. (a) 0, (b) 5, (c) 10, and (d) 15 sccm.

concentration increased to 5 and 10 sccm. However, as the oxygen concentration increased to 15 sccm, the grains become more nonuniform. Additionally, the oxygen vacancies are the dominant factor for the current transmission paths and were generated during the sputtering process. The oxygen reacts with Sm target materials and parts of the oxygen might fill oxygen vacancies, which will break the current transmission paths and also cause the variation of the X value in SmO_X. Hence, too much oxygen will fill oxygen vacancies and cause the decrease in the number of oxygen vacancies, which will affect the number of current transmission paths and also the insulating properties of the SmO_X layer, probably suggesting that the optimal oxygen concentration is 10 sccm. The cross-sectional image of the proposed RRAM is shown in Fig. 4. Clearly, the thicknesses of the Al top electrode and SmO_X layer are about 179 and 35 nm, respectively.

During the RF sputtering process, defects and oxygen vacancies of as-deposited SmO_X thin films were filled and compensated by oxygen. For the I–V characteristics shown in Fig. 5, by sweeping the bias to negative over the set voltage, a gradual increase in current was presented to switch the cells from the HRS to the LRS (set process). Additionally, the cell turns back to HRS on applying a larger positive bias than the reset voltage (reset process). Moreover, it can be found that all the RRAMs exhibit clear bipolar behaviors, and all the on/off ratios of both SET and RESET states are greater than 102. Furthermore, it exhibited less than 3 V operating voltage and good memory switching properties.

It was reported that oxygen contents play an important role in the resistive switching of RRAM devices.[16–18] In the filament model, the formation and rupture of the conducting filaments are the main switching mechanisms. Since the switching properties of the SmO_X film are highly correlated with the number of oxygen ions and vacancies within the electrode and thin film, the oxygen concentration will play an important role in the resistive switching phenomenon of this SmO_X RRAM device.

For RRAMs, many models had been suggested to illustrate their conductive mechanisms in the past, such as the modification of Schottky barrier height by trapped charge carriers,[19] constitution of a conductive filamentary path,[20] migration of oxygen vacancies,[21] and carriers tunneling between crystalline defects.[22] Furthermore, many more researchers have attempted to optimize the resistive switching properties of RRAMs. The two most popular

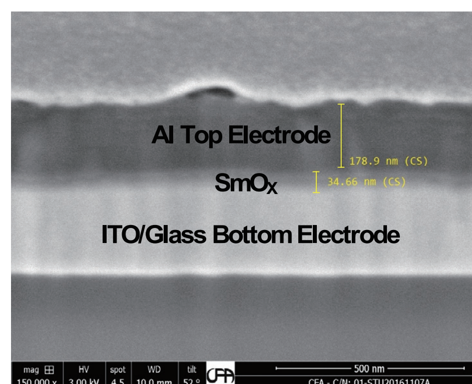

Fig. 4. (Color online) Cross-sectional image of SmO_X thin films (RF power = 75 W, O_2 = 10 sccm).

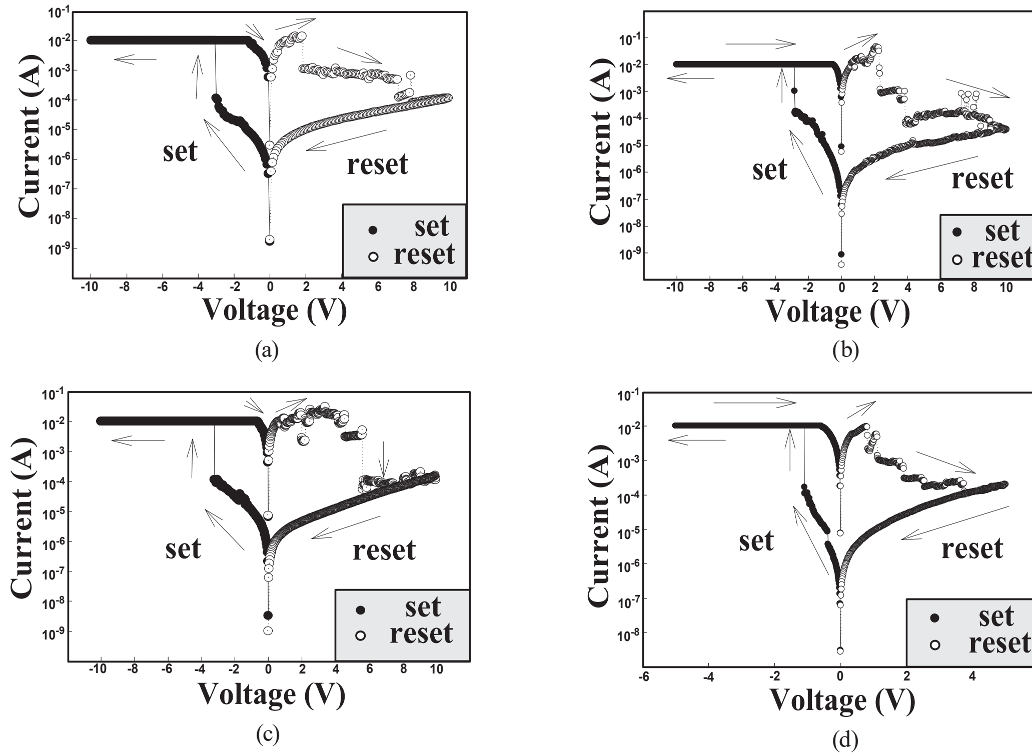

Fig. 5. I–V characteristics of Al/SmO_X/ITO RRAM for different oxygen concentrations (RF power = 75 W). (a) 0, (b) 5, (c) 10, and (d) 15 sccm.

conductive mechanisms of RRAMs are the ohmic conduction [Eq. (1)] and the space charge limit conduction (SCLC) behaviors [Eq. (2)].(23) As the RF power was 75 W, Fig. 6 shows the current–voltage characteristics of 0, 5, 10, and 15 sccm O_2 Al/SmO_X/ITO RRAMs in terms of Ln(I) and Ln(V). We can observe that as the operating voltages were low, the current conduction mechanism was ohmic conduction behavior (external electric field dominated, slope ≈ 1) for both SET and RESET states. However, for higher operating voltages, decreasing current can be observed owing to parts of defects filled by the carriers. Thus, parts of conduction mechanisms will change to SCLC behavior (slope ≈ 2). However, for intermediate operating voltage (1 < slope < 2), the conduction mechanisms were composed of both ohmic conduction as well as SCLC.

$$J = nq\mu E \exp\left(\frac{-\Delta E_{ac}}{kT}\right), \tag{1}$$

$$J = \frac{9\varepsilon_i \mu V^2}{8d^3}. \tag{2}$$

Here, J is current density, n is electron concentration, μ is mobility of electrons, E is applied electric field, ΔE_{ac} is the activation energy of electrons, k is Boltzmann's constant, ε_i is insulator dynamic permittivity, d is the thickness of the insulator layer, and V is applied voltage.

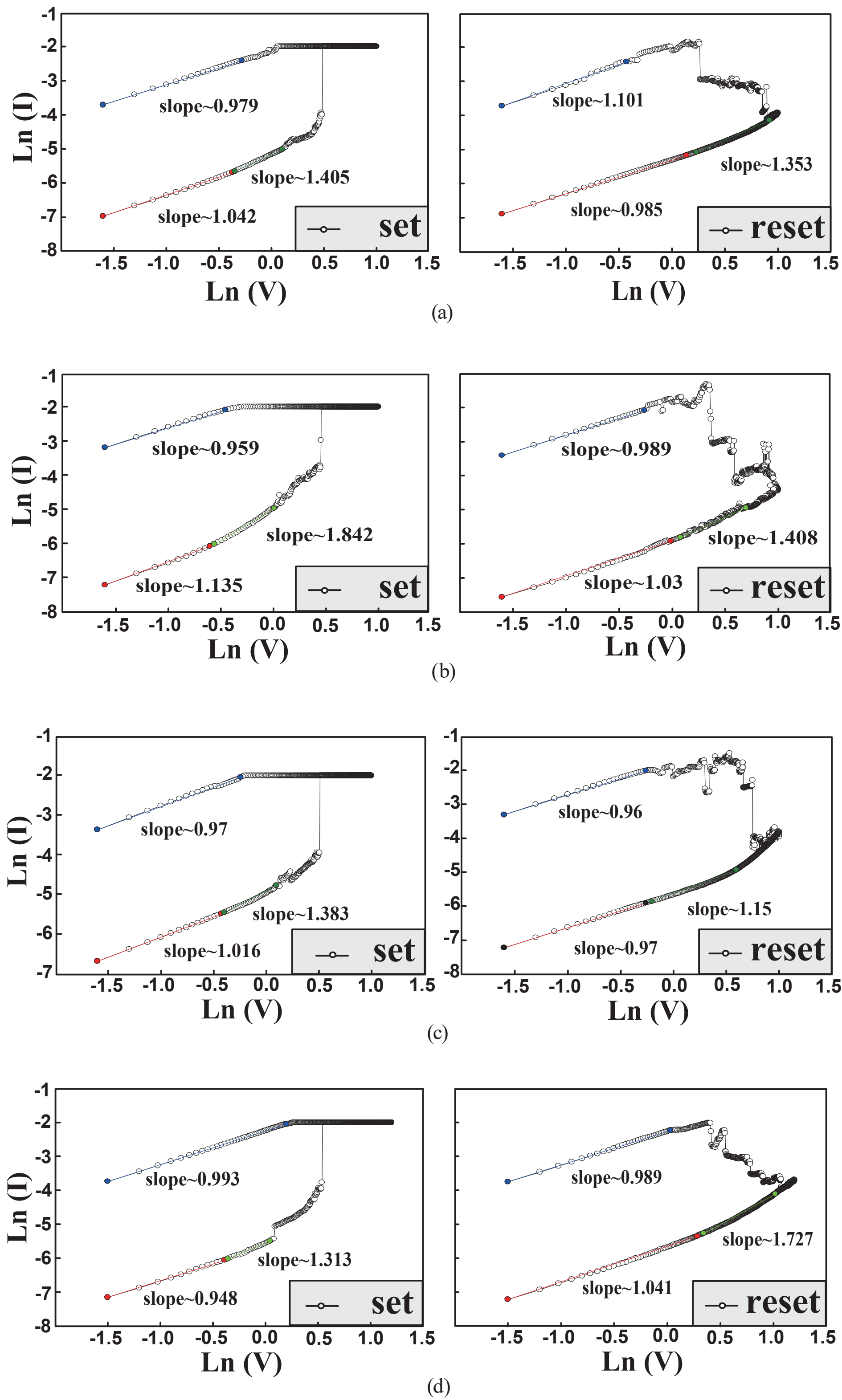

Fig. 6. (Color online) Ln(I)–Ln(V) plots of Al/SmO_X/ITO RRAM for different oxygen concentrations (RF power = 75 W). (a) 0, (b) 5, (c) 10, and (d) 15 sccm.

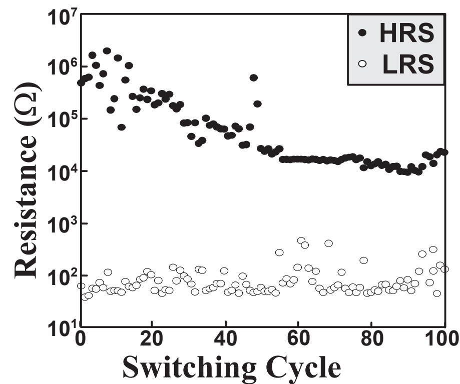

Fig. 7. Switching cycle of the Al/SmO_X/ITO RRAM (RF power = 75 W, O_2 = 10 sccm).

As the RF power is 75 W and the oxygen concentration is 10 sccm, the switching endurance characteristics of the Al/SmO_X/ITO RRAM were measured and shown in Fig. 7. There was a slight fluctuation of resistance in the HRS (resistance is about 10^4–10^6 Ω) and LRS (resistance is about 10^2 Ω) states. Thus, the device reveals stable bipolar switching properties and greater than 10^2 HRS/LRS resistance ratio even after 100 continuous switching cycles. It indicates the good endurance properties and nonvolatile memory applications for these Al/SmO_X/ITO RRAM devices.

4. Conclusions

In conclusion, the resistive switching electrical properties of thin-film Al/SmO_X/ITO RRAMs were investigated and demonstrated. In addition, as the RF power is 75 W and the oxygen concentration is 10 sccm, the RRAM devices exhibited stable bipolar behavior of greater than 10^2 on/off current ratio, good memory window, and good memory reliability of 100 switching cycles. As the operating voltage is low, the conduction mechanisms for low- and high-resistance states are dominated by ohmic conduction behavior for both SET and RESET states. However, as a higher operating voltage is applied, parts of conduction mechanisms will change to SCLC behaviors. The high uniformity and low-power operation in the Al/SmO_X/ITO RRAMs are promising for high-density and low-power electronic applications.

Acknowledgments

This work was kindly supported by the Ministry of Science and Technology of the Republic of China (MOST 106-2221-E-218-034 and MOST 105-2221-E-218-034).

References

1 G. I. Meijer: Science **319** (2008) 1625.
2 K. M. Kim, D. S. Jeong, and C. S. Hwang: Nanotechnology **22** (2011) 254002.
3 C. H. Ho, C. L. Hsu, C. C. Chen, J. T. Liu, C. S. Wu, C. C. Huang, C. Hu, and F. L. Yang: Tech. Dig. Int. Electron Devices Meet. (2010) 19.1.1.

4 R. Waser and M. Aono: Nat. Mater. **6** (2007) 833.
5 S. Z. Rahaman and S. Maikap: Microelectron. Reliab. **50** (2010) 643.
6 S. J. Choi, J. H. Lee, H. J. Bae, W. Y. Yang, T. W. Kim, and K. H. Kim: IEEE Electron Device Lett. **30** (2009) 120.
7 L. Goux, K. Opsomer, R. Degraeve, R. Müller, C. Detavernier, D. J. Wouters, M. Jurczak, L. Altimime, and J. A. Kittl: Appl. Phys. Lett. **99** (2011) 053502.
8 Y. Bernard, P. Gonon, and V. Jousseaume: Appl. Phys. Lett. **96** (2010) 193502.
9 Y. Tsuji, T. Sakamoto, N. Banno, H. Hada, and M. Aono: Appl. Phys. Lett. **96** (2010) 023504.
10 K. Tsunoda, Y. Fukuzumi, J. R. Jameson, Z. Wang, P. B. Griffin, and Y. Nishi: Appl. Phys. Lett. **90** (2007) 113501.
11 H. Choi, M. Pyun, T. W. Kim, M. Hasan, R. Dong, J. Lee, J. B. Park, J. Yoon, D. J. Seong, T. Lee, and H. Hwang: IEEE Electron Device Lett. **30** (2009) 302.
12 S. H. Jo, K. H. Kim, and W. Lu: Nano Lett. **9** (2009) 870.
13 A. K. Kulkarnia, K. H. Schulzb, T. S. Lima, and M. Khanb: Thin Solid Films **308–309** (1997) 1.
14 F. E. Akkad, M. Marafi, A. Punnoose, and G. Prabu: Phys. Status Solidi A **77** (2000) 445.
15 S. K. Choi and J. I. Lee: J. Vac. Sci. Technol. A **19** (2001) 2043.
16 M. Fujimoto, H. Koyama, M. Konagai, Y. Hosoi, K. Ishihara, S. Ohnishi, and N. Awaya: Appl. Phys. Lett. **89** (2006) 223509.
17 S. Seo, M. J. Lee, D. H. Seo, E. J. Jeoung, D. S. Suh, Y. S. Joung, I. K. Yoo, I. R. Hwang, S. H. Kim, I. S. Byun, J. S. Kim, J. S. Choi, and B. H. Park: Appl. Phys. Lett. **85** (2004) 5655.
18 D. C. Kim, M. J. Lee, S. E. Ahn, S. Seo, J. C. Park, I. K. Yoo, I. G. Baek, H. J. Kim, E. K. Yim, J. E. Lee, S. O. Park, H. S. Kim, U. I. Chung, J. T. Moon, and B. I. Ryu: Appl. Phys. Lett. **88** (2006) 232106.
19 T. Oka and N. Nagaosa: Phys. Rev. Lett. **95** (2005) 266403.
20 B. J. Choi, D. S. Jeong, S. K. Kim, C. Rohde, S. Choi, J. H. Oh, H. J. Kim, C. S. Hwang, K. Szot, R. Waser, B. Reichenberg, and S. Tiedke: J. Appl. Phys. **98** (2005) 033715.
21 S. H. Jeon, B. H. Park, J. Lee, B. Lee, and S. Han: Appl. Phys. Lett. **89** (2006) 042904.
22 M. J. Rozenberg, I. H. Inoue, and M. J. Sanchez: Appl. Phys. Lett. **88** (2006) 033510.
23 S. M. Sze: Physics of Semiconductor Devices (Wiley, New York, 1981) 2nd ed., p. 403.